



Swansea University  
Prifysgol Abertawe



## Cronfa - Swansea University Open Access Repository

---

This is an author produced version of a paper published in:

*Biosensors and Bioelectronics*

Cronfa URL for this paper:

<http://cronfa.swan.ac.uk/Record/cronfa50808>

---

### Paper:

Teixeira, S., Abreu, C., Parkes, L., Davies, J., Yao, S., Sawhney, M., Margarit, L., Gonzalez, D., Pinto, I., et. al. (2019). Direct monitoring of breast and endometrial cancer cell epigenetic response to DNA methyltransferase and histone deacetylase inhibitors.. *Biosensors and Bioelectronics*, 111386

<http://dx.doi.org/10.1016/j.bios.2019.111386>

Released under the terms of a Creative Commons Attribution Non-Commercial No Derivatives License (CC-BY-NC-ND).

---

This item is brought to you by Swansea University. Any person downloading material is agreeing to abide by the terms of the repository licence. Copies of full text items may be used or reproduced in any format or medium, without prior permission for personal research or study, educational or non-commercial purposes only. The copyright for any work remains with the original author unless otherwise specified. The full-text must not be sold in any format or medium without the formal permission of the copyright holder.

Permission for multiple reproductions should be obtained from the original author.

Authors are personally responsible for adhering to copyright and publisher restrictions when uploading content to the repository.

<http://www.swansea.ac.uk/library/researchsupport/ris-support/>

# Accepted Manuscript

Direct monitoring of breast and endometrial cancer cell epigenetic response to DNA methyltransferase and histone deacetylase inhibitors.

S.R. Teixeira, C.M. Abreu, L. Parkes, J. Davies, S. Yao, M.A. Sawhney, L. Margarit, D. Gonzalez, I. Mendes Pinto, L.W. Francis, R.S. Conlan



PII: S0956-5663(19)30465-8

DOI: <https://doi.org/10.1016/j.bios.2019.111386>

Article Number: 111386

Reference: BIOS 111386

To appear in: *Biosensors and Bioelectronics*

Received Date: 11 April 2019

Revised Date: 23 May 2019

Accepted Date: 30 May 2019

Please cite this article as: Teixeira, S.R., Abreu, C.M., Parkes, L., Davies, J., Yao, S., Sawhney, M.A., Margarit, L., Gonzalez, D., Pinto, I.M., Francis, L.W., Conlan, R.S., Direct monitoring of breast and endometrial cancer cell epigenetic response to DNA methyltransferase and histone deacetylase inhibitors., *Biosensors and Bioelectronics* (2019), doi: <https://doi.org/10.1016/j.bios.2019.111386>.

This is a PDF file of an unedited manuscript that has been accepted for publication. As a service to our customers we are providing this early version of the manuscript. The manuscript will undergo copyediting, typesetting, and review of the resulting proof before it is published in its final form. Please note that during the production process errors may be discovered which could affect the content, and all legal disclaimers that apply to the journal pertain.

2  
3 **Direct monitoring of breast and endometrial cancer cell epigenetic response to DNA**  
4 **methyltransferase and histone deacetylase inhibitors.**

5  
6  
7 **Authors**

8  
9 S. R. Teixeira<sup>2,3</sup>, C. M. Abreu<sup>4</sup>, L. Parkes<sup>1,3</sup>, J. Davies<sup>1,3</sup>, S. Yao<sup>1,3</sup>, M. A. Sawhney<sup>1,3</sup>, L. Margarit<sup>1,5</sup>, D.  
10 Gonzalez<sup>1,3</sup>, I. Mendes Pinto<sup>4</sup>, L. W. Francis<sup>1,3</sup>, R. S. Conlan<sup>1,3,\*</sup>

11  
12 **Affiliations**

13 <sup>1</sup>Swansea University Medical School, Singleton Park, Swansea, SA2 8PP, UK

14 <sup>2</sup>College of Engineering, Swansea University, Bay Campus, Swansea, SA1 8QQ, UK

15 <sup>3</sup>Centre for NanoHealth, Swansea University, Singleton Park, Swansea, SA2 8PP, UK

16 <sup>4</sup>International Iberian Nanotechnology Laboratory (INL), Portugal

17 <sup>5</sup>Abertawe Bro Morgannwg University Health Board, Princess of Wales Hospital Bridgend, UK.

18 \* corresponding author, r.s.conlan@swansea.ac.uk

19  
20 **Keywords**

21 epigenetics; EIS; DNA methylation; histone acetylation; cancer cell lines  
22  
23  
24  
25  
26  
27  
28  
29  
30  
31  
32  
33

38 function and tumorigenesis. Therapeutic strategies based on DNA methyltransferase (DNMT) and histone  
39 deacetylase (HDAC) inhibitors are currently in use and under development for the treatment of cancers.  
40 Genome-wide DNA methylation profiling has been proposed for use in disease diagnosis, and histone  
41 modification profiling for disease stratification will follow suit. However, whether epigenome sequencing  
42 technologies will be feasible for rapid clinic diagnosis and patient treatment monitoring remains to be seen,  
43 and alternative detection technologies will almost certainly be needed. Here we used electrochemical  
44 impedance spectroscopy (EIS) employing a graphene-based screen-printed electrode system to directly  
45 measure global DNA methylation and histone H3 acetylation to compare non-cancer and breast cancer cell  
46 lines. We demonstrated that whilst global methylation was not useful as a differential marker in the  
47 cellular systems tested, histone H3 acetylation was effective at higher chromatin levels. Using breast and  
48 endometrial cancer cell models, EIS was then used to monitor cellular responses to the DNMT and HDAC  
49 inhibitors 5-Aza-2'-deoxycytidine and suberoylanilide hydroxamic acid *in vitro*, and proved very effective  
50 at detecting global cellular responses to either treatment, indicating that this approach could be useful in  
51 following treatment response to epigenetic drugs. Moreover, this work reports the first combined analysis  
52 of two epigenetic markers using a unified graphene-based biosensor platform, demonstrating the potential  
53 for multiplex analysis of both methylation and acetylation on the same sample.

## 54 55 **1. Introduction**

56  
57 Cancer cells undergo epigenetic changes in 5-methylcytosine distribution that include global DNA  
58 hypomethylation and the hypermethylation of promoter CpG islands associated with tumor-suppressor  
59 genes. DNA methylation is just one facet in the coordinated regulation of chromatin structure that also  
60 involves discrete modifications to histone proteins, including histone H3 and H4 deacetylation, among  
61 others, which collectively result in transcriptionally altered states (Capp, 2017; Jones and Baylin, 2007; Lo  
62 and Zhou, 2018; Sheahan and Ellis, 2018).

63  
64 Large-scale epigenomic studies have been made possible using established complex technologies. These  
65 allow the genome-wide mapping of epigenetic marks, including DNA methylation and histone  
66 modifications, which are critical for regulating gene expression. In turn, we are learning how mapping  
67 aberrant alterations to these epigenetic marks can be used in clinical diagnostics (Bock et al., 2016; Butler  
68 and Dent, 2013; Libertini et al., 2016; Rendeiro et al., 2016).

69  
70 DNA methylation and histone modification biomarkers have several advantages that qualify them for  
71 broad use as *in vitro* diagnostics and to support clinical decisions: (i) They can be cell-type-specific, yet  
72 robust toward transient perturbations. (ii) They are binary marks (i.e., for a single cell and allele, an  
73 epigenetic mark is either modified or not), which facilitates reliable measurements on heterogeneous  
74 samples. (iv) The use of epigenetic markers to detect cancer sensitively is based on the premise that tumor-  
75 derived chromatin/DNA is released into bodily fluids, or other remote samples, and can be detected by  
76 abnormal DNA methylation and histone modification patterns (Bormann et al., 2018; Coleman and De,  
77 2018; Graff-Baker et al., 2018; Singh et al., 2018; Xi et al., 2018; Zhang et al., 2018).

78  
79 Current approaches to assess the epigenetic state currently target individual genetic loci to determine  
80 histone modification (predominantly acetylation and methylation) and DNA methylation status. Bisulphite  
81 sequencing has been the mainstay of DNA methylation analysis with methylated and hydroxymethylated  
82 DNA immunoprecipitation (MeDIP and (h)MeDIP) methods coming online, whilst chromatin  
83 immunoprecipitation (ChIP) is the research tool of choice for determining histone modifications. However,

include serum proteomics using mass spectrometry that whilst progressing in clinical feasibility studies, require expensive and highly technical hardware, and expert users for sample and data analysis.

Electrochemical immunosensors using advances in nanomaterials are being developed for biosensing applications (Zhu et al., 2015). For the detection of epigenetic modifications electrochemical analytical methods offer several advantages over other techniques, such as surface plasmon resonance and atomic force spectroscopy, in terms of sensitivity, simplicity and portability (Stewart and Tsui, 2018). Furthermore, they offer limits of detection of methylated DNA within the levels reported to be found circulating in plasma (Stewart and Tsui, 2018). In addition, instrumentation required to make such measurements is low-cost, with instrument refinement reducing costs even further (Sawhney and Conlan, 2019). Gold and carbon -based electrode systems remain the most utilized working electrode materials, despite many other materials having been evaluated (Krejцова et al., 2017), and have been used in screen printed formats that offer low cost per unit, and do not require extensive preparation to obtain a pristine surface prior to use. Graphene as a working electrode offers a high signal to noise ratio, and is easily functionalized with antibodies when coated with polyaniline, which also serves a conductive polymer and is used as an additive transducer layer to avoid the introduction of graphene surface defects (Gazze et al., 2018; Teixeira et al., 2014a). Graphene offers a further advantage over gold electrodes for the detection and quantification of DNA as it lacks the inherent absorption properties for unmodified DNA that are displayed by gold surfaces due to affinity interactions (Koo et al., 2015). Here, we demonstrate the use of a graphene-based immunosensor, where anti-5-methylcytosine (anti-5mc) and anti-acetylated histone H3 (anti-acH3) antibodies were directly coupled to a polyaniline-modified screen-printed graphene electrode to detect DNA and chromatin using label-free EIS measurements. Using this system global levels of methylated DNA and histone H3 acetylated chromatin levels were assessed in normal (MCF12A) and cancer (MCF7) breast cell models, and MCF7 and HEC50 cells treated with a DNMT or HDAC inhibitors were found to show alterations in DNA methylation or histone H3 acetylation respectively. Overall, this study highlights the effectiveness EIS graphene immune sensors for the direct label- and amplification-free detection of global epigenetic modifications in cancer cells, and thus their potential for monitoring therapeutic efficacy.

## 2. Materials and Methods

**Cell culture and treatments.** MCF7 cells (ATCC, Maryland USA) were cultured in Eagle's Minimum Essential Medium (Gibco, ThermoFisher Scientific, UK) supplemented with 10% (v/v) foetal bovine serum (Gibco) and 0.01mg/ml insulin (Sigma-Aldrich, Missouri, USA). Hec50 cells (ATCC, Maryland USA) were cultured in Dulbecco's Modified Eagle Medium: Nutrient Mixture F-12 (DMEM/F12) (Gibco, ThermoFisher Scientific, UK) supplemented with 10% (v/v) fetal bovine serum (Gibco), 1% (v/v) penicillin and streptomycin (Gibco), sodium bicarbonate and sodium pyruvate. MCF12A cells (ATCC, Maryland USA) were cultured in Dulbecco's Modified Eagle Medium: Nutrient Mixture F-12 (DMEM/F12) (Gibco, ThermoFisher Scientific, UK) supplemented with 5% (v/v) horse serum (Gibco), 20ng/ml human epidermal growth factor, 100 ng/ml cholera toxin, 0.01 mg/ml bovine insulin and 500 ng/ml hydrocortisone 95%. All cell lines were grown at 37°C in a humidified atmosphere with 5% CO<sub>2</sub> to 90% confluency in T75 flasks (Corning, New York, USA) before collection. Cells were grown to 40% or 60% confluency respectively before exchanging full growth media for stripped media prior to treatment with the DNMT inhibitor 5-Aza-2'-deoxycytidine (1 µM), suberoylanilide hydroxamic acid (2.5 µM) or vehicle (DMSO).

136  
137 **Immunosensor assembly.** Graphene-SPEs were purchased from DropSens (DRP-110GPH Metrohm UK  
138 Ltd, Runcorn, UK) and were composed of a carbon counter electrode, a silver pseudo-reference electrode,  
139 and a printed graphene working electrode (4 mm  $\varnothing$ ). Electrical characterization of SPEs was performed by  
140 connecting the SPEs to the potentiostat/galvanostat *via* a suitable switch box (DropSens, Metrohm UK Ltd,  
141 Runcorn, UK). In order to mediate selective immunodetection of chromatin and gDNA to the graphene  
142 sensor surface, PANI functionalization was utilized, as previously described (Teixeira et al., 2014b).

143  
144 **Electrochemical measurements.** CV and EIS were performed using a Metrohm Autolab PGSTAT302N  
145 equipped with FRA32M and DRP-DSC connector; control and analysis were provided through Nova  
146 software version 2.0.1 and higher (Metrohm UK Ltd, Runcorn, UK). CV procedures spanned -0.7 to 0.7  
147 Volts starting and ending at 0V with a scan rate of 0.05 Volts per second. EIS procedures applied 50  
148 frequencies between 1000 and 0.01 hertz, logarithmically distributed at an amplitude of 0.01 V<sub>RMS</sub> on a DC  
149 bias of 0.1V with the reference electrode. EIS data was fitted to a R(C[R(RC)]) equivalent circuit model  
150 using a maximum of 300 iterations with weight factor applied.

151  
152 **Chromatin/gDNA detection and quantification.** The functionalized biosensing platforms are based on  
153 impedance measurements resulting in changes of resistivity (Rct) following the binding of a chromatin  
154 or gDNA to the specific antibody immobilized on the sensor surface. Increasing concentrations of  
155 chromatin ranging from 0.0086 to 134 ng/ $\mu$ L for MCF12A, 0.0078 to 123 ng/ $\mu$ L for MCF7 and 0.0053 to  
156 416 ng/ $\mu$ L for Hec50; and gDNA solutions, ranging from 0.0048 to 75 ng/ $\mu$ l for all cell lines, were  
157 prepared by dilution of 1708 ng/ $\mu$ L of chromatin and 75 ng/ $\mu$ L of gDNA stock solutions in media.

158 **Chromatin immunoprecipitation.** ChIP assays were performed using the Chromatrap® ChIP-seq kit  
159 following the manufacturers' instructions (Porvair Sciences Ltd, Wrexham, UK). Chromatin was  
160 quantified by Nanodrop 2000 (ThermoFisher Scientific) and visualized using by agarose gel  
161 electrophoresis to ensure correct distribution of fragment sizes prior to immunoprecipitation. 1  $\mu$ g of each  
162 chromatin sample was used per ChIP with 2  $\mu$ g of relevant antibody; anti acetyl H3 antibody (Millipore,  
163 Darmstadt, Germany) or non-specific rabbit IgG (Chromatrap, Porvair Sciences Ltd, Wrexham, UK).  
164 qPCR was carried on the target gene *p21 forward primer* 5'-CCCACAGCAGAGGAGAAAGAA; *reverse*  
165 *primer* 5'-CTGGAAATCTCTGCCAGACA.

166 **Methylated DNA immunoprecipitation.** MeDIP assays were carried out using the Chromatrap MeDIP kit  
167 according to the manufacturers' protocol (Porvair Sciences Ltd, Wrexham, UK). gDNA was quantified by  
168 Nanodrop 2000 (ThermoFisher Scientific) and visualized using agarose gel electrophoresis to ensure  
169 correct distribution of fragment sizes prior to immunoprecipitation. 500 ng DNA was used per MeDIP with  
170 1 $\mu$ g kit supplied anti-5-methylcytosine antibody or non-specific mouse IgG and linker. Samples were  
171 neutralized, and amplification of enriched methylated DNA carried out at the *CXCL12 locus forward*  
172 *primer* 5'-CTCATTTCAGTTCCCGCCATC; *reverse primer* 5'-GCCGCTTATTGTCCCTGTG.

173 **Western blotting.** Total protein was extracted using RIPA buffer and quantified using the DC Protein  
174 assay (BioRad, Watford, UK). Relevant protein concentrations were separated by SDS PAGE. Proteins  
175 were transferred to PVDF membrane, blocked and probed with a 1/15,000 dilution of anti-acetyl H3  
176 antibody (Millipore, Watford, UK) followed by ECL anti-rabbit IgG horse radish peroxidase (GE

179 **Dot blotting:** gDNA extracted and sheared as described for the MEDIP protocol was used for dot blotting.  
180 Immun-Blot PVDF Membrane (BioRad, Watford, UK) was activated with methanol and equilibrated with  
181 transfer buffer prior to spotting the membrane with 100ng heat denatured gDNA. A 1/300 dilution of the  
182 primary antibody anti-5mC (Chromatrap Porvair Sciences Ltd, Wrexham, UK) was used to probe the  
183 methylated DNA and detected with ECL anti-rabbit IgG horse radish peroxidase (GE Healthcare, Bucks,  
184 UK).

### 185 3. Results

#### 186 *Immunosensor assembly and functionalization*

187  
188 Electrochemical impedance spectroscopy (EIS) is a label and amplification free technique that enables  
189 direct molecular measurements on modified surface electrodes (Sánchez et al., 2008). Here, we adapted  
190 our previously reported screen-printed electrode (SPE)-graphene/polyaniline (PANI) platform to detect  
191 methylated DNA and acetylated histone H3 using anti-5mC and anti-acH3 antibodies respectively. Sensor  
192 optimization using control DNA and chromatin extracted from cell line models established sensitivity  
193 according to our established protocols (Teixeira et al., 2016).  
194

195  
196 Sensor assembly was evaluated using scanning electron microscopy and atomic force microscopy (Fig.  
197 S1), and electron transfer properties determined against a redox probe and evaluated by cyclic  
198 voltammetry (CV) and EIS. Unmodified graphene-SPEs showed a quasi-reversible electrochemical  
199 response for the  $[\text{Fe}(\text{CN})_6]^{3-/4-}$  redox couple with  $\Delta E_p$  of 0.158 V and  $\Delta I_p$  of 0.285 mA, respectively. After  
200 10 cycles, the modification of graphene-SPE surface with PANI resulted in a  $\Delta I_p$  increase of 0.894 mA  
201 and a  $\Delta E_p$  decrease of 2.898 V (Fig. 1A) attributed to positively charged amino groups of the PANI  
202 molecule attracting the negative charge of  $[\text{Fe}(\text{CN})_6]^{3-/4-}$  promoting electron transfer on the electrode  
203 surface (Zor et al., 2013). A cyclic voltammogram of the SPE-graphene/PANI/Antibody electrode showed  
204 a decrease peak-to-peak potential separation ( $\Delta E_p$  of 0.547 V). Further, addition of the BSA blocking  
205 agent to the SPE-graphene/PANI/Ab electrode surface gave rise to a change on the electrochemical  
206 behavior of  $[\text{Fe}(\text{CN})_6]^{3-/4-}$ , leading to a  $\Delta E_p$  increase of 0.258 V and decreased  $\Delta I_p$  value of 0.546 mA.  
207 BSA molecules cause masking of the electrode surface oxidation/reduction of the redox probe  $[\text{Fe}(\text{CN})_6]^{3-}$   
208  $/4-$  (Daniels and Pourmand, 2007).  
209

210 EIS data are presented as Nyquist plots where the  $R_{ct}$  at the electrode surface is given by the semicircle  
211 diameter obtained in EIS and can be used to define the interface properties of the electrode. The  
212 unmodified graphene surface display fast electron-transfer properties ( $R_{ct} = 884 \Omega$ , Fig. 1B), which  
213 increases following PANI deposition ( $R_{ct} = 1.13 \text{ K}\Omega$ , Fig. 1B). Following covalent attachment of anti-  
214 acH3 antibody, the  $R_{ct}$  increased to 1.82  $\text{K}\Omega$  (Fig. 1B), demonstrating that electron exchange between the  
215 redox probe and the electrode was impeded, and this was enhanced further when BSA was added to the  
216 SPE-graphene/PANI/Ab ( $R_{ct} = 2.09 \text{ K}\Omega$ , Fig. 1B). Similar data was obtained for the anti-5mC antibody  
217 sensor platform build (Fig. 1C and D). To define linear ranges for 5mC and acH3 concentrations,  $R_{ct}$   
218 values of genomic DNA (gDNA; 4.8pg/ $\mu\text{L}$  - 75ng/ $\mu\text{L}$ ) and chromatin (8.6pg/ $\mu\text{L}$  - 134ng/ $\mu\text{L}$ ) were  
219 determined (Fig. 2A and B respectively).  
220

#### 221 *DNA methylation and histone H3 acetylation status in normal and breast cancer cell models*

220  $\Omega \pm 205 \Omega$ , 75 ng/ $\mu$ L input gDNA) (Fig. 3A), consistent with global methylated DNA assessment made  
221 using dot blotting (Fig. 3B). Single locus analysis of a CpG island in the 5'UTR of CXCL12, which  
222 encodes the stromal cell derived factor 1 $\alpha$  protein commonly overexpressed in many cancers (Guo et al.,  
223 2016), also demonstrated that DNA methylation levels were similar in both normal and cancer breast cell  
224 types (Fig. 3C).

231  
232 EIS also enabled direct measurement of global histone H3 acetylation (acH3) in MCF7 cells for e.g.,  
233 4460  $\Omega \pm 50 \Omega$ , 134 ng/ $\mu$ L input chromatin which was significantly higher than the levels measured in  
234 MCF12A (3287  $\Omega \pm 589 \Omega$ , 75 ng/ $\mu$ L input chromatin) (Fig. 3D), and this difference was confirmed by  
235 protein blotting (Fig. 3E). Conversely ChIP analysis at the cyclin dependent kinase inhibitor 1 (p21) locus  
236 revealed an 8-fold lower level in acetylation in MCF7 compared to MCF12A cells (Fig. 3F),  
237 demonstrating that whilst globally the MCF7 genome is hyperacetylated compared to MCF12A cells, there  
238 are also locus specific and therefore functional differences between these breast cancer cell types.  
239 Suppression of p21 expression through loss of acetylation results in loss of cell cycle arrest, driving  
240 proliferation, a hallmark of cancer cells, and is therefore expected in the cancer cell line.

241  
242 EIS sensor measurements show that global measurement of epigenetic marks can be useful in  
243 differentiating cancer and non-cancer cell types, and that combining epigenetic signatures may be  
244 beneficial. For example, MCF7 (low methylation + high acetylation) can be distinguished from MCF12A  
245 (low methylation + low acetylation). With the addition of other epigenetic marks an algorithm could be  
246 developed to provide a cell specific signature.

#### 247 248 ***Monitoring global response to decitabine and vorinostat treatments in cancer cell lines.***

249  
250 Small chemical modifications that trigger chromatin remodeling through processes including DNA  
251 methylation and histone acetylation are of increasing interest as therapeutic targets in cancer diseases due  
252 to reversible nature of these epigenetic modifications (Dawson and Kouzarides, 2012; Flavahan et al.,  
253 2017). For example, 5-Aza-2'-deoxycytidine (decitabine) is a strong inducer of DNA de-methylation and is  
254 approved for the treatment of myelodysplastic syndrome (Mossman et al., 2010; Ramos et al., 2015), and  
255 suberoylanilide hydroxamic acid (vorinostat) is a histone deacetylase inhibitor (HDACi) approved for the  
256 treatment of cutaneous T cell lymphoma (Qu et al., 2017). The rapid detection of global epigenetic status  
257 could represent a useful tool for risk assessment, diagnosis, and for treatment monitoring, complementing locus  
258 specific analysis of tumor suppressor and oncogene epigenetic status in patients.

259  
260 EIS was used to assess MCF7 and HEC50 cells for response to decitabine and vorinostat treatments (Fig. 4A  
261 and D; Fig. 5A and D). The response of MCF7 cells to decitabine was readily distinguished using EIS  
262 sensors at higher concentrations of input gDNA ( $\geq 15$ ng/ $\mu$ L). For example, a  $\Delta\Omega$  between untreated  
263 (2630  $\Omega \pm 160 \Omega$  at 75 ng/ $\mu$ L) compared to treated (2130 $\Omega \pm 122 \Omega$  at 75ng/ $\mu$ L) was -500 $\Omega$  showing an  
264 expected decrease in DNA following treatment. For endometrial cancer cells a similar trend was observed,  
265 for example a mean  $\Delta\Omega$  of -780 at 75ng/ $\mu$ L (Fig. 5A).

266  
267 These responses were validated using a methylated DNA specific dot blot, where 100ng total gDNA  
268 extracted from both MCF7 and HEC50 cells showed decreased intensity following treatment (Fig. 4B and  
269 5B), and by MeDIP where the CpG island region of the CXCL12 gene was significantly demethylated. A



Acetylated histone H3 was similarly analyzed following exposure of cells to vorinostat. Significantly increased acetylation was observed in the treated samples compared to untreated controls in both MCF7 and HEC50 with  $\Delta\Omega$  much greater compared to that observed for decitabine treatment (Fig. 4D and 5D). For MCF7, a  $\Delta\Omega$  of +653 ( $8173 \Omega \pm 99 \Omega$  treated,  $7520 \Omega \pm 331 \Omega$  untreated) was measured in MCF7 at the highest input chromatin concentration of 24.6 ng/ $\mu$ L for untreated and 44 ng/ $\mu$ L for vorinostat treated, indicative of an increase in open chromatin architecture. For Hec50, a  $\Delta\Omega$  of +4600 was ( $7830 \Omega \pm 90 \Omega$  treated,  $3230\Omega \pm 38 \Omega$  untreated) was obtained for 83.2 ng/ $\mu$ L for untreated cells and 58 ng/ $\mu$ L for treated cells).

Immunosensor performance was also validated by western blotting (Fig. 4E and 5E), and p21 ChIP where a 2.11 and 3.28 -fold increase in H3 acetylation following vorinostat treatment were measured in MCF7 and HEC50 respectively (Fig. 4F and 5F).

The use of EIS in monitoring cellular responses to drug treatment is clearly very effective, and such a monitoring would be of value in determining patient responses to such treatments, particularly if measurements could be made directly from free circulating methylated DNA and modified chromatin that are known to alter in patients.

#### 4. Discussion

The adaptation of a graphene based EIS immunosensor has enabled for the first-time direct amplification-free and label-free detection of both DNA- and nucleosome- linked epigenetic modifications. The method developed here utilizes antibodies that have been validated and widely used for locus specific genome wide analysis associated with CHIP- and MeDIP- techniques, making comparison between EIS and epigenomic analysis more robust. The EIS method presents a snapshot of 'gross' epigenetic status rather than the 'statically global view' obtained from the assimilation of multi-loci epigenome datasets. The speed of signal acquisition compared to PCR or DNA sequencing is substantially improved as there is no requirement for template amplification. Furthermore, the relative simplicity of the analytical process and very low sample volumes lend this approach to clinical utility. This technology is envisioned to become a price competitive point-of-care system, where single use functional screen-printed electrodes are preferable to reusable systems due to the need to minimize false positive results that would likely occur due to incomplete biological sample removal from the biosensor surface. Future miniaturization of this technology, as printing techniques become more refined and with higher resolution, will go some way to reducing the associated waste stream. Current legislation necessitates that clinical samples are correctly handled of therefore sensor chips exposed to clinical material must be disposed of appropriately.

Cytosine methylation and gross histone H3 acetylation are regulatory mechanisms for, and established markers of, transcription repression and activation respectively. DNA methylation directs gene silencing through the establishment of condensed heterochromatic structures, whereas histone H3 acetylation results in the loss of association between lysine residues in histone tails and the negatively charged phosphate backbone of DNA resulting in transition to a euchromatic state. Furthermore, both mechanisms are the target of currently available therapeutics including decitabine, a cytosine analogue that functions as a DNA methylase transferase (DNMT) inhibitor. Following its incorporation into DNA during replication, decitabine irreversibly binds to DNMT1, sequestering it the site of interaction and rendering it ineffective.

321 Here we have reported differences between EIS measurements as a  $\Delta\Omega$  value, as the exact amount of DNA  
322 or chromatin present has not been directly determined. However, as total global DNA methylation levels  
323 are estimated to be 0.7 – 2.8 mole percent i.e., moles of 5-methyl cytosine per 100 bases of total DNA in  
324 eukaryotes (Hall, 1971), we estimate for example that 0.52-2.1ng/ $\mu$ L methylated DNA per 75ng/ $\mu$ L input  
325 DNA is being detected in the EIS assay. Similarly, it is estimated that only 1.2% of chromatin is acetylated  
326 at histone H3 (Roh et al., 2005), therefore we are detecting approximately 1.6 ng/ $\mu$ L acetylated histone H3  
327 per 134ng/ $\mu$ L input chromatin.

328  
329 DNA methylation levels were similar for normal and breast cancer cell lines tested using EIS suggesting  
330 that global methylation without any selection of genetic loci is not useful in differentiating between the cell  
331 types used in this study. In contrast, the level of global acetylation in the MCF7 cancer cell line was higher  
332 than in the non-cancer MCF12A cells illustrating that, even in the absence of any pharmacological  
333 treatment that can modify cellular epigenetic status, differences can be determined between cell types that  
334 originate from the same tissue.

335  
336 Using EIS sensors we were able to trace cellular response to treatments with DNMT or HDAC inhibitors,  
337 monitoring the respective decreases in DNA methylation or increases in histone H3 acetylation. The  
338 response of both breast and endometrial cancer cells to decitabine and vorinostat was as expected with  
339 differentiation between cell responses to either treatment detectable at detectable very low levels of input  
340 DNA or chromatin. With this detection platform available it will now be possible to monitor patient  
341 responses to treatment directly from patient samples.

342  
343 With the recent surge in global efforts to map epigenomes across cancer types and patient cohorts (Bock et  
344 al., 2016; Libertini et al., 2016; Rendeiro et al., 2016; Xi et al., 2018) it is becoming possible to associate  
345 global epigenetic changes with disease status using statistical approaches. We propose that multiplex EIS  
346 could be used to simultaneously assess several epigenetics marks, and that such an approach could  
347 accurately diagnose and even stage disease progression directly from patient samples. Such an approach  
348 would obviate the need for DNA sequencing or indeed the complex and ongoing processes of identifying  
349 and characterizing circulating protein biomarkers. The use of a multi-epigenetic marker algorithm coupled  
350 with the  $\Delta\Omega$  differential quantification against known and predetermined/preprogrammed standards  
351 provides an obvious and compelling strategy that now needs to be exploited.

## 352 353 354 **5. Conclusions**

355  
356 Whilst a number of DNA methylation sensors have been reported (Krejcová et al., 2017) no single  
357 platform has yet emerged as a preferred solution for accurate and rapid methylation testing. The use of  
358 biosensors in monitoring changes in global methylation levels in response to cancer cell treatment with  
359 decitabine is reported here for the first time. The development of biosensors for detection of histone  
360 acetylation lags significantly behind that of DNA methylation biosensors, and has to date been limited to  
361 fluorescent based approaches (Wang et al., 2017). The system presented in the current study uses an  
362 antibody-based approach, and employs the same platform used for DNA methylation detection. Using this  
363 system, we were able to demonstrate for the first-time the amplification and label free immuno-detection  
364 of histone H3 acetylation, and monitor responses of breast and endometrial cancer models to vorinostat, a  
365 drug that has undergone clinical trials for the treatment of advanced breast cancer (Luu et al., 2018). The

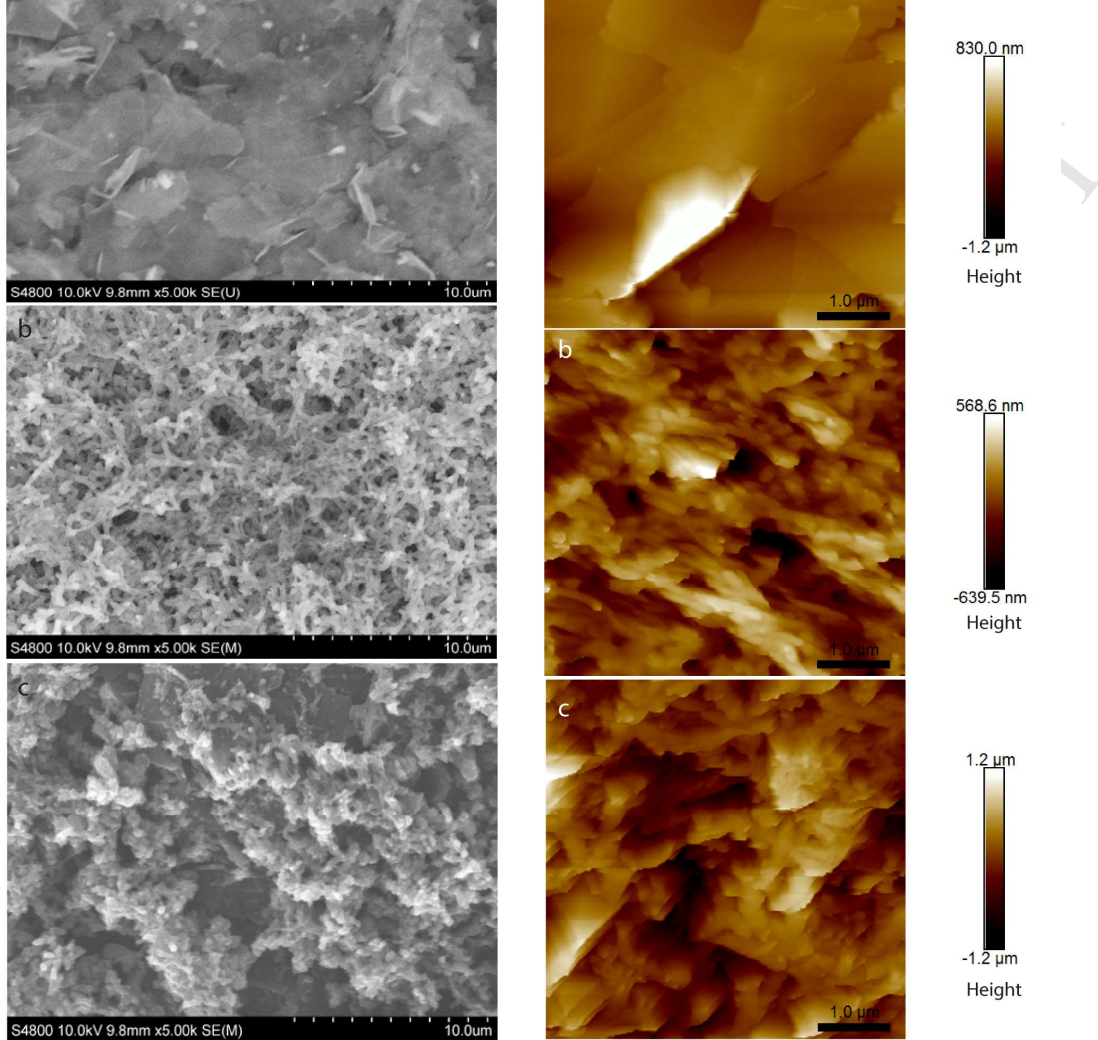
369 The combined detection of two different epigenetic marks, using a unified detection platform, now opens  
370 the way to monitoring multiple epigenetic modifications, particularly targeting the multitude of  
371 modifications that occur on histone proteins, which as well as acetylation, include protein methylation,  
372 ubiquitylation, phosphorylation, sumoylation, ribosylation and citrullination. Developments in smaller,  
373 multiplexed sensors are now required, and could result in a move from SPEs to emerging FET-based  
374 systems (Campos et al., 2019).

### 375 **Acknowledgments**

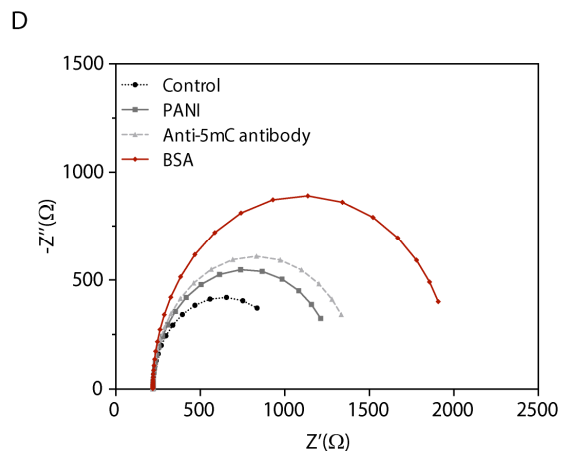
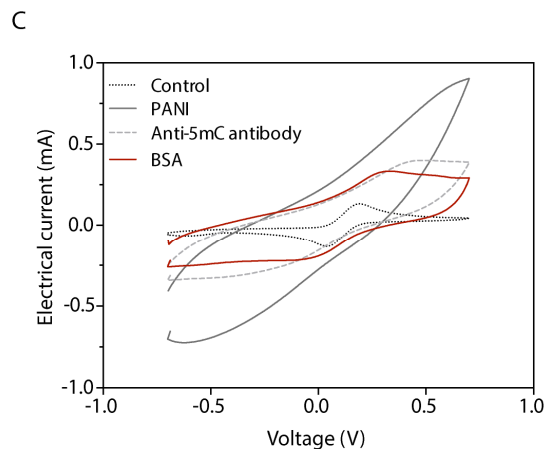
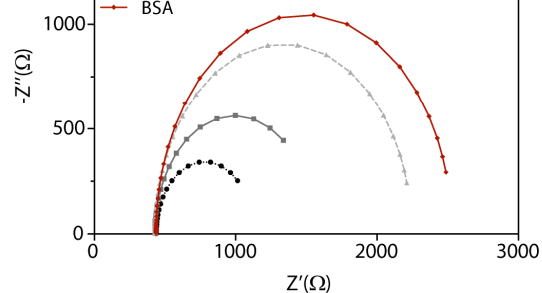
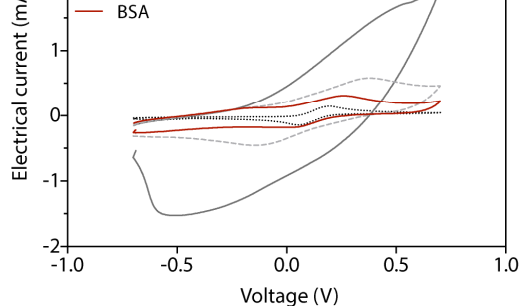
376 **Funding:** S.T. Welsh National Research Network in Advanced Engineering and Materials (NRNF77).  
377 I.M.P. Marie Curie COFUND Programme “NanoTRAINforGrowth” from the European Union’s Seventh  
378 Framework Programme for research, technological development and demonstration under grant agreement  
379 no 600375. This article is a result of the project Advancing cancer research: from basic knowledge to  
380 application (NORTE-01-0145-FEDER-000029), co-financed by Norte Portugal Regional Operational  
381 Programme (NORTE 2020), under the PORTUGAL 2020 Partnership Agreement, through the European  
382 Regional Development Fund (ERDF).

383 **Author contributions:** S.R.T. study design, sensor design, fabrication and data collection. L.P. and J.D.  
384 ChIP and MeDIP and data analysis. C.M.A. data analysis, figure and manuscript preparation. S.Y. and  
385 A.S. sensor fabrication, data collection, data analysis. L.M. expert clinical input in manuscript preparation.  
386 I.M.P. sensor design and fabrication, data analysis, manuscript preparation. D.G. study design, manuscript  
387 preparation. L.W.F. study concept and design, manuscript preparation. R.S.C. study concept and design,  
388 manuscript preparation.

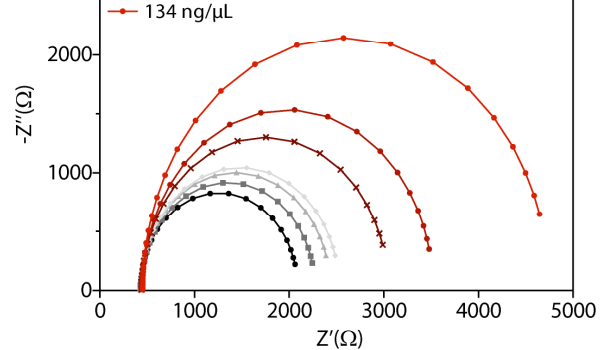
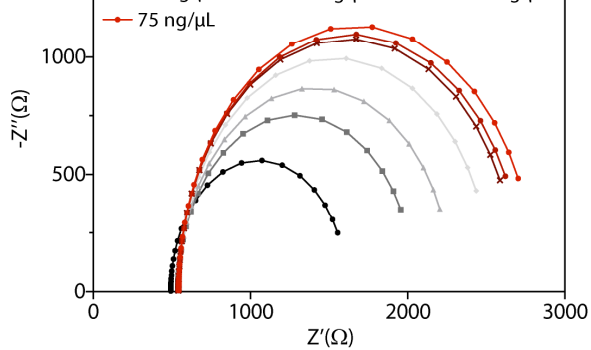
389 **Competing interests:** The authors declare that they have no competing interests.  
390  
391



393  
 394 **Fig. S1. Surface characterization of biosensor assembly.** (A) Scanning Electron Microscopy of (a) unmodified  
 395 graphene; (b) graphene modified with PANI (C); anti-ach3 attached to the PANI layer; (B) Atomic Force  
 396 Microscopy of (a) unmodified graphene; (b) graphene modified with PANI (c); anti-ach3 attached to the PANI layer.

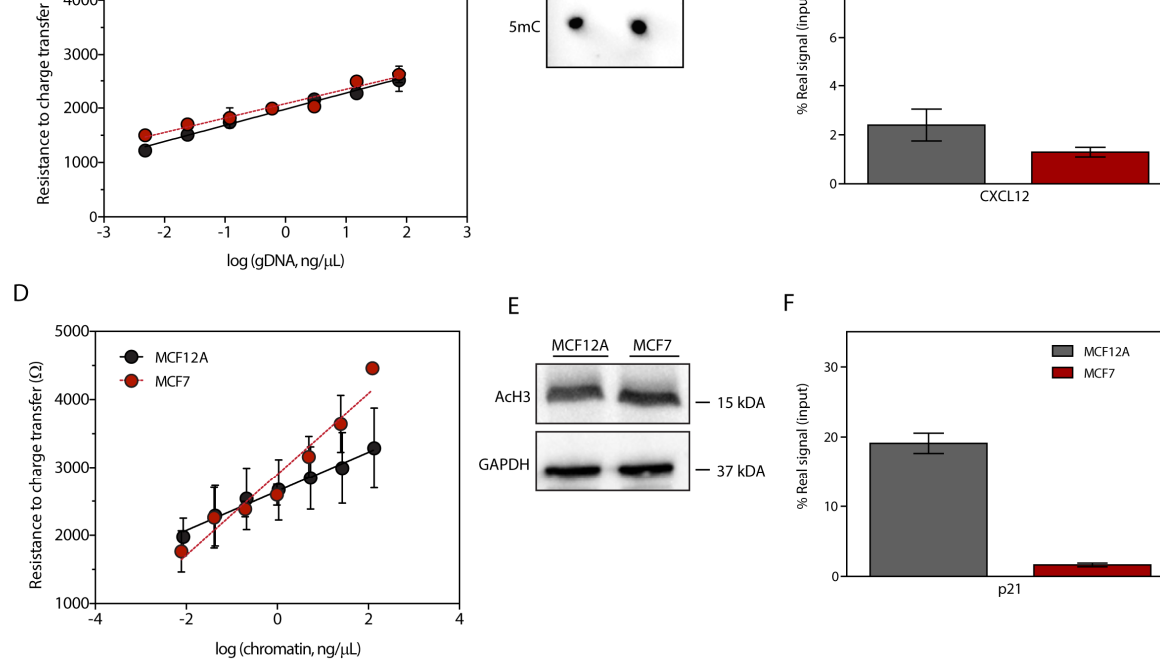


397  
398 **Fig 1. Electrochemical characterization of biosensor assembly.** (A) Cyclic voltammogram (CV) of the acetylation  
399 immunosensor assembly after each modification of graphene-SPE/PANI/anti-acH3/BSA. (B) Nyquist plots of  
400 graphene-SPE/PANI/anti-acH3/BSA sensor, obtained in 5.0mM  $[\text{Fe}(\text{CN})_6]^{3-/4-}$  PBS buffer pH 7.4. (C) CV of the  
401 methylation immunosensor assembly after each modification of graphene-SPE/PANI/anti-5mC/BSA (D) Nyquist  
402 plots of graphene-SPE/PANI/anti-5mC/BSA sensor, obtained in 5.0mM  $[\text{Fe}(\text{CN})_6]^{3-/4-}$  PBS buffer pH 7.4.  
403



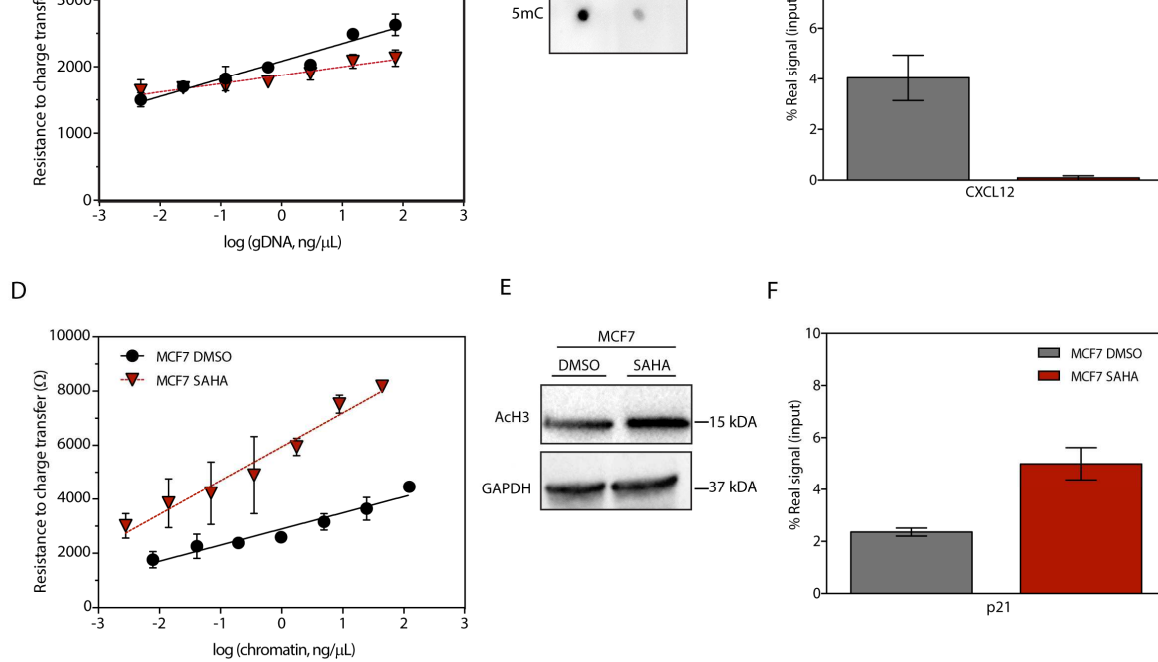
404  
 405 **Fig. 2. Global epigenetic modifications in breast cells (MCF12A).** (A) Representative Nyquist plot of the  
 406 methylation biosensor upon detection of increasing concentrations of gDNA (B) Representative Nyquist plot of the  
 407 acetylation biosensor upon detection of increasing concentrations of chromatin.

ACCEPTED MANUSCRIPT



408  
409

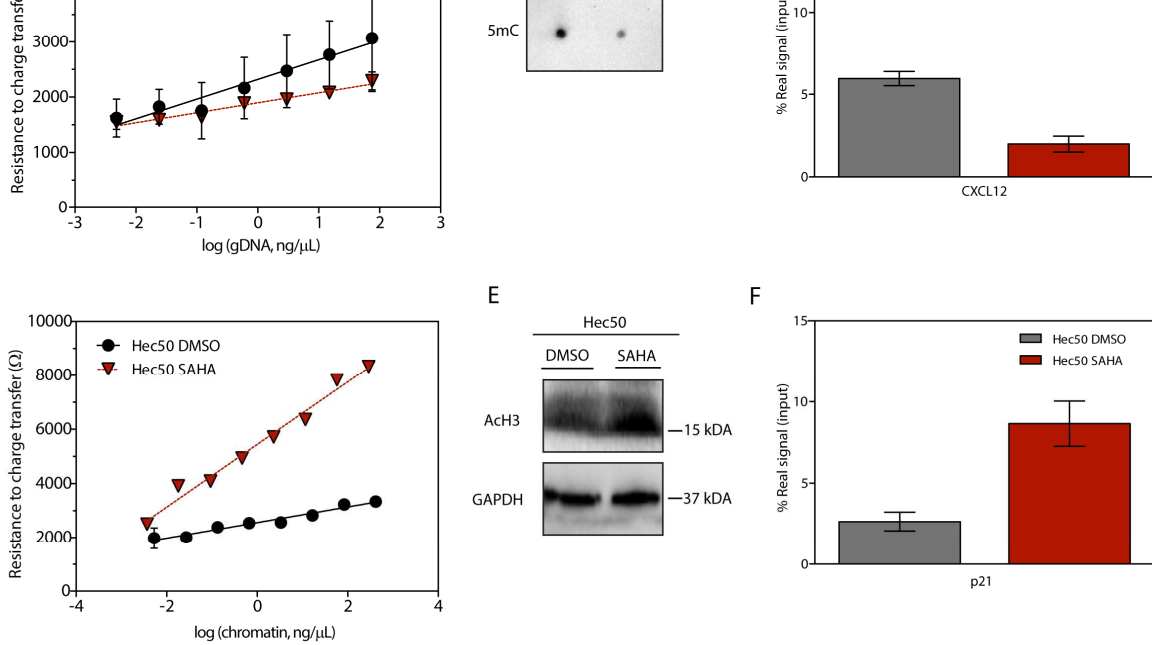
410 **Fig. 3. Detection of global (A, B, D and E) and locus (C and F) modifications in breast cancer cells.** (A)  
411 Calibration curve, plotting log(gDNA) against Rct for MCF12A and MCF7. Error bars represent the standard error of  
412 the mean of three biological replicates. (B) Dot blotting of global methylation for MCF12A versus MCF7 using  
413 gDNA with anti-5mC antibody. (C) MeDIP enrichment of CXCL12 from 500 ng MCF12A and MCF7 gDNA by  
414 MeDIP using anti-5mC antibody relative to a non-specific IgG reported as % real signal (% positive antibody - %  
415 IgG, relative to a standard gDNA input sample). Error bars represent the standard error of the mean of three  
416 biological replicates. (D) Calibration curve, plotting log(chromatin) against Rct for MCF12A and MCF7. Error bars  
417 represent the standard error of the mean of three biological replicates. (E) Western blot detection of global acetylated  
418 histone H3 (acH3) in MCF12A and MCF7 chromatin using a specific antibody directed against the modified histone  
419 protein. (F) Enrichment of the human p21 locus associated with acetylated histone H3 by ChIP using 1  $\mu$ g MCF12A  
420 and MCF7 chromatin. Error bars represent the standard error of the mean of three biological replicates.



421

422 **Fig. 4. Detection of global (A, B, D and E) and locus (C and F) modifications in breast cancer cells (MCF7)**  
 423 **upon treatment.** (A) Calibration curve, plotting log(gDNA) against Rct for MCF7 treated versus MCF7 untreated.  
 424 Error bars represent the standard error of the mean of three biological replicates. (B) Dot blotting of global  
 425 methylation for MCF7 treated versus untreated using gDNA with anti-5mC antibody. (C) MeDIP enrichment of  
 426 CXCL12 from 500 ng MCF7 treated and MCF7 untreated gDNA using anti-5mC antibody relative to a non-specific  
 427 IgG. Error bars represent the standard error of the mean of three biological replicates. (D) Calibration curve, plotting  
 428 log(chromatin) against Rct for MCF7 treated versus MCF7 untreated. Error bars represent the standard error of the  
 429 mean of three biological replicates. (E) Western blot detection of global acetylated histone 3 (acH3) in MCF7 treated  
 430 versus untreated chromatin using a specific antibody directed against the modified histone protein. (F) Enrichment of  
 431 the human p21 locus associated with acetylated histone H3 by ChIP using 1 μg MCF7 treated and MCF7 untreated  
 432 chromatin. Error bars represent the standard error of the mean of three biological replicates.  
 433





434

435 **Fig. 5. Detection of global (A, B, D and E) and locus (C and F) modifications in endometrial cells (Hec50) upon**  
 436 **treatment. (A)** Calibration curve, plotting log(gDNA) against Rct for Hec50 treated versus Hec50 untreated. Error  
 437 bars represent the standard error of the mean of three biological replicates. **(B)** Dot blotting of global methylation for  
 438 Hec50 treated versus Hec50 untreated using gDNA with anti-5mC antibody. **(C)** MedIP enrichment of CXCL12  
 439 from 500 ng Hec50 treated and untreated gDNA by MedIP using anti-5mC antibody relative to a non-specific IgG  
 440 demonstrates. Error bars represent the standard error of the mean of three biological replicates. **(D)** Calibration curve,  
 441 plotting log(chromatin) against Rct for Hec50 treated versus Hec50 untreated. Error bars represent the standard error  
 442 of the mean of three biological replicates. **(E)** Western blot detection of global acetylated histone 3 (acH3) in Hec50  
 443 treated versus Hec50 untreated chromatin using a specific antibody directed against the modified histone protein. **(F)**  
 444 Enrichment of the human p21 locus associated with acetylated histone H3 by ChIP using 1  $\mu$ g Hec50 treated  
 445 untreated chromatin. Error bars represent the standard error of the mean of three biological replicates.  
 446  
 447

452 Aiki, Dooner, R., Dasato, F., Campai, M., Dam, C., Danneke, C.M., Diep, D., Fernandez, A.I.,  
453 Gerhauser, C., Haake, A., Heilmann, K., Holcomb, T., Hussmann, D., Ito, M., Kläver, R., Kreutz, M.,  
454 Kulis, M., Lopez, V., Nair, S.S., Paul, D.S., Plongthongkum, N., Qu, W., Queirós, A.C., Reinicke, F.,  
455 Sauter, G., Schlomm, T., Statham, A., Stirzaker, C., Strogantsev, R., Urdinguio, R.G., Walter, K.,  
456 Weichenhan, D., Weisenberger, D.J., Beck, S., Clark, S.J., Esteller, M., Ferguson-Smith, A.C., Fraga,  
457 M.F., Guldberg, P., Hansen, L.L., Laird, P.W., Martín-Subero, J.I., Nygren, A.O.H., Peist, R., Plass,  
458 C., Shames, D.S., Siebert, R., Sun, X., Tost, J., Walter, J., Zhang, K., 2016. Quantitative comparison  
459 of DNA methylation assays for biomarker development and clinical applications. *Nat. Biotechnol.*  
<https://doi.org/10.1038/nbt.3605>

460 Bormann, F., Rodríguez-Paredes, M., Lasitschka, F., Edelman, D., Musch, T., Benner, A., Bergman, Y.,  
461 Dieter, S.M., Ball, C.R., Glimm, H., Linhart, H.G., Lyko, F., 2018. Cell-of-Origin DNA Methylation  
462 Signatures Are Maintained during Colorectal Carcinogenesis. *Cell Rep.*  
463 <https://doi.org/10.1016/j.celrep.2018.05.045>

464 Butler, J.S., Dent, S.Y.R., 2013. The role of chromatin modifiers in normal and malignant hematopoiesis.  
465 *Blood.* <https://doi.org/10.1182/blood-2012-10-451237>

466 Campos, R., Borme, J., Guerreiro, J.R., Machado, G., Cerqueira, M.F., Petrovykh, D.Y., Alpuim, P., 2019.  
467 Attomolar label-free detection of dna hybridization with electrolyte-gated graphene field-effect  
468 transistors. *ACS Sensors* 4, 286–293. <https://doi.org/10.1021/acssensors.8b00344>

469 Capp, J.P., 2017. Tissue disruption increases stochastic gene expression thus producing tumors: Cancer  
470 initiation without driver mutation. *Int. J. Cancer.* <https://doi.org/10.1002/ijc.30596>

471 Coleman, N., De, S., 2018. Mutation Signatures Depend on Epigenomic Contexts. *Trends Cancer* 4, 659–  
472 661.

473 Daniels, J.S., Pourmand, N., 2007. Label-free impedance biosensors: Opportunities and challenges.  
474 *Electroanalysis.* <https://doi.org/10.1002/elan.200603855>

475 Dawson, M.A., Kouzarides, T., 2012. Cancer Epigenetics: From Mechanism to Therapy. *Cell* 150, 12–27.

476 Flavahan, W.A., Gaskell, E., Bernstein, B.E., 2017. Epigenetic plasticity and the hallmarks of cancer.  
477 *Science* (80- ). <https://doi.org/10.1126/science.aal2380>

478 Gazze, A., Ademefun, R., Conlan, R.S., Teixeira, S.R., 2018. Electrochemical impedance spectroscopy  
479 enabled CA125 detection; toward early ovarian cancer diagnosis using graphene biosensors. *J.*  
480 *Interdiscip. Nanomedicine* 3, 82–88. <https://doi.org/10.1002/jin2.40>

481 Graff-Baker, A.N., Orozco, J.I.J., Marzese, D.M., Salomon, M.P., Hoon, D.S.B., Goldfarb, M., 2018.  
482 Epigenomic and Transcriptomic Characterization of Secondary Breast Cancers. *Ann. Surg. Oncol.*  
483 <https://doi.org/10.1245/s10434-018-6582-7>

484 Guo, F., Wang, Y., Liu, J., Mok, S.C., Xue, F., Zhang, W., 2016. CXCL12/CXCR4: A symbiotic bridge  
485 linking cancer cells and their stromal neighbors in oncogenic communication networks. *Oncogene.*  
486 <https://doi.org/10.1038/onc.2015.139>

487 Hall, R.H., 1971. *The modified nucleosides in nucleic acids.* Columbia University Press (1971).

488 Jones, P.A., Baylin, S.B., 2007. The Epigenomics of Cancer. *Cell* 128, 683–692.

489 Koo, K.M., Sina, A.A.I., Carrascosa, L.G., Shiddiky, M.J.A., Trau, M., 2015. DNA-bare gold affinity  
490 interactions: Mechanism and applications in biosensing. *Anal. Methods.*  
491 <https://doi.org/10.1039/c5ay01479d>

492 Krejcova, L., Richtera, L., Hynek, D., Labuda, J., Adam, V., 2017. Current trends in electrochemical  
493 sensing and biosensing of DNA methylation. *Biosens. Bioelectron.* 97, 384–399.  
494 <https://doi.org/10.1016/J.BIOS.2017.06.004>

- 499 Lo, P.K., Zhou, Q., 2018. Emerging Techniques in Single-Cell Epigenomics and their Applications to  
500 Cancer Research. *J. Clin. Genomics* 1, 1–8.
- 501 Luu, T., Kim, K. pyo, Blanchard, S., Anyang, B., Hurria, A., Yang, L., Beumer, J.H., Somlo, G., Yen, Y.,  
502 2018. Phase IB trial of ixabepilone and vorinostat in metastatic breast cancer. *Breast Cancer Res.*  
503 *Treat.* 167, 469–478. <https://doi.org/10.1007/s10549-017-4516-x>
- 504 Mossman, D., Kim, K.T., Scott, R.J., 2010. Demethylation by 5-aza-2'-deoxycytidine in colorectal cancer  
505 cells targets genomic DNA whilst promoter CpG island methylation persists. *BMC Cancer.*  
506 <https://doi.org/10.1186/1471-2407-10-366>
- 507 Qu, K., Zaba, L.C., Satpathy, A.T., Giresi, P.G., Li, R., Jin, Y., Armstrong, R., Jin, C., Schmitt, N.,  
508 Rahbar, Z., Ueno, H., Greenleaf, W.J., Kim, Y.H., Chang, H.Y., 2017. Chromatin Accessibility  
509 Landscape of Cutaneous T Cell Lymphoma and Dynamic Response to HDAC Inhibitors. *Cancer*  
510 *Cell.* <https://doi.org/10.1016/j.ccell.2017.05.008>
- 511 Ramos, M.P., Wijetunga, N.A., McLellan, A.S., Suzuki, M., Grealley, J.M., 2015. DNA demethylation by  
512 5-aza-2'-deoxycytidine is imprinted, targeted to euchromatin, and has limited transcriptional  
513 consequences. *Epigenetics and Chromatin.* <https://doi.org/10.1186/s13072-015-0004-x>
- 514 Rendeiro, A.F., Schmidl, C., Strefford, J.C., Walewska, R., Davis, Z., Farlik, M., Oscier, D., Bock, C.,  
515 2016. Chromatin accessibility maps of chronic lymphocytic leukaemia identify subtype-specific  
516 epigenome signatures and transcription regulatory networks. *Nat. Commun.*  
517 <https://doi.org/10.1038/ncomms11938>
- 518 Roh, T.Y., Cuddapah, S., Zhao, K., 2005. Active chromatin domains are defined by acetylation islands  
519 revealed by genome-wide mapping. *Genes Dev.* <https://doi.org/10.1101/gad.1272505>
- 520 Sánchez, S., Roldán, M., Pérez, S., Fàbregas, E., 2008. Toward a fast, easy, and versatile immobilization  
521 of biomolecules into carbon nanotube/polysulfone-based biosensors for the detection of hCG  
522 hormone. *Anal. Chem.* <https://doi.org/10.1021/ac7025282>
- 523 Sawhney, M., Conlan, R., 2019. POISED-5, a Portable On-board Electrochemical Impedance  
524 Spectroscopy Biomarker Analysis Device. *Biomed Microdevices.*  
525 <https://doi.org/https://doi.org/10.1007/s10544-019-0406-9>
- 526 Sheahan, A. V, Ellis, L., 2018. Epigenetic reprogramming: A key mechanism driving therapeutic  
527 resistance. *Urol Oncol* 36, 375–379.
- 528 Singh, A.A., Petraglia, F., Nebbioso, A., Yi, G., Conte, M., Valente, S., Mandoli, A., Scisciola, L.,  
529 Lindeboom, R., Kerstens, H., Janssen-Megens, E.M., Pourfarzad, F., Habibi, E., Berentsen, K., Kim,  
530 B., Logie, C., Heath, S., Wierenga, A.T.J., Clarke, L., Flicek, P., Jansen, J.H., Kuijpers, T., Yaspo,  
531 M.L., Della Valle, V., Bernard, O., Gut, I., Vellenga, E., Stunnenberg, H.G., Mai, A., Altucci, L.,  
532 Martens, J.H.A., 2018. Multi-omics profiling reveals a distinctive epigenome signature for high-risk  
533 acute promyelocytic leukemia. *Oncotarget.* <https://doi.org/10.18632/oncotarget.25429>
- 534 Stewart, C.M., Tsui, D.W.Y., 2018. Circulating cell-free DNA for non-invasive cancer management.  
535 *Cancer Genet.* <https://doi.org/10.1016/j.cancergen.2018.02.005>
- 536 Teixeira, S., Conlan, R.S., Guy, O.J., Sales, M.G.F., 2014a. Label-free human chorionic gonadotropin  
537 detection at picogram levels using oriented antibodies bound to graphene screen-printed electrodes. *J.*  
538 *Mater. Chem. B* 2, 1852–1865. <https://doi.org/10.1039/c3tb21235a>
- 539 Teixeira, S., Conlan, R.S., Guy, O.J., Sales, M.G.F., 2014b. Label-free human chorionic gonadotropin  
540 detection at picogram levels using oriented antibodies bound to graphene screen-printed electrodes. *J.*  
541 *Mater. Chem. B* 2, 1852. <https://doi.org/10.1039/c3tb21235a>
- 542 Teixeira, S.R., Lloyd, C., Yao, S., Andrea Salvatore Gazze, Whitaker, I.S., Francis, L., Conlan, R.S.,

546 fluorometric biosensor for label-free and homogenous detection of protein acetylation-related  
547 enzymes activities. *Biosens. Bioelectron.* 91, 400–407. <https://doi.org/10.1016/j.bios.2016.12.065>

548 Xi, Y., Shi, J., Li, Wenqian, Tanaka, K., Allton, K.L., Richardson, D., Li, J., Franco, H.L., Nagari, A.,  
549 Malladi, V.S., Coletta, L. Della, Simper, M.S., Keyomarsi, K., Shen, J., Bedford, M.T., Shi, X.,  
550 Barton, M.C., Lee Kraus, W., Li, Wei, Dent, S.Y.R., 2018. Histone modification profiling in breast  
551 cancer cell lines highlights commonalities and differences among subtypes. *BMC Genomics*.  
552 <https://doi.org/10.1186/s12864-018-4533-0>

553 Zhang, J., Han, X., Gao, C., Xing, Y., Qi, Z., Liu, R., Wang, Y., Zhang, X., Yang, Y.G., Li, X., Sun, B.,  
554 Tian, X., 2018. 5-Hydroxymethylome in Circulating Cell-free DNA as A Potential Biomarker for  
555 Non-small-cell Lung Cancer. *Genomics, Proteomics Bioinforma.*  
556 <https://doi.org/10.1016/j.gpb.2018.06.002>

557 Zhu, C., Yang, G., Li, H., Du, D., Lin, Y., 2015. Electrochemical sensors and biosensors based on  
558 nanomaterials and nanostructures. *Anal. Chem.* <https://doi.org/10.1021/ac5039863>

559 Zor, E., Hatay Patir, I., Bingol, H., Ersoz, M., 2013. An electrochemical biosensor based on human serum  
560 albumin/graphene oxide/3-aminopropyltriethoxysilane modified ITO electrode for the  
561 enantioselective discrimination of d- and l-tryptophan. *Biosens. Bioelectron.*  
562 <https://doi.org/10.1016/j.bios.2012.10.068>

563

methylation and histone H3 acetylation levels. The system application demonstrated global alterations in DNA methylation or histone H3 acetylation in response to treatment with decitabine and vorinostat respectively.

- System application demonstrated global alterations in DNA methylation or histone H3 acetylation in response to treatment with decitabine and vorinostat respectively.
- Results were corroborated using established techniques including CHIP and MeDIP.
- The study opens up the opportunity for assessing point-of-care monitoring of patient responses to epigenetic therapeutics, and multiplexing epigenetic marker detection on a unified platform.

ACCEPTED MANUSCRIPT

J.D. Resources; Formal analysis

C.M.A. Validation; Writing - original draft; Writing - review & editing

S.Y. Resources; Software; Validation

A.S. Resources; Software; Validation

L.M. Conceptualization; Writing - review & editing

I.M.P. Conceptualization; Investigation; Supervision; Validation; Visualization; Writing - original draft; Writing - review & editing

D.G. Conceptualization; Supervision; Writing - original draft; Writing - review & editing

L.W.F. Conceptualization; Writing - original draft; Writing - review & editing

R.S.C. Conceptualization; Funding acquisition; Supervision; Writing - original draft; Writing - review & editing

ACCEPTED MANUSCRIPT